ICMIEE18-249

Numerical Study on Aero-Acoustic Behavior for Flow over a Supercritical Airfoil at Low Reynolds Number

Syed Angkan Haider, Tanveer Islam Joy, Md. Fazlur Rahman Akanda

Department of Mechanical Engineering, Bangladesh University of Engineering & Technology, Dhaka-1000, BANGLADESH

ABSTRACT

A two-dimensional supercritical RAE-2822 airfoil cross-section with 100 mm chord length was analyzed at low Reynolds number (Re) flow and the resulting aero-acoustic parameters were investigated. A Reynolds number of approximately 168,000 (based on airfoil chord length) was used for the analysis. The study was conducted for three different angles of attack, namely 0^0, 6^0 and 12^0. For the computational analysis, 2-D transient Reynolds Averaged Navier-Stokes (RANS) equations were used, coupled with the two equation *k-ω* shear stress transport (SST) turbulence model and broadband noise source settings. The pressure, turbulent intensity, acoustic power level and LEE self- and shear-noise were analyzed in the vicinity of the airfoil surface and wake; possible explanations behind noise generation and their relation to turbulence, flow separation and vortex formation at different angles of attack were discussed. It was observed that the aero-acoustic noise increased with angle of attack as the vorticity and turbulence effects got stronger.

Keywords: Supercritical airfoil, Reynolds number, shear-noise, self-noise.

1. Introduction

Aircraft noise has become a major concern because of its detrimental effects on communities living in the vicinity of airports while also registering itself as a significant loss of energy during flight. Aerodynamic noise is one of the most important sources of aircraft noise arising from the airflow around the airfoil. This becomes more noticeable when aircrafts fly at low altitudes near the airports. This noise, while being a loss in the flow, is also known to be a health hazard, with many different physical and psychological effects. So knowledge about acoustic noise is vital for being able to not just find how it is produced but also possible ways on how it can be minimized.

Sandberg *et al.* [1] conducted DNS of the flow at low Re around NACA-0006 and NACA-0012 airfoils and studied airfoil self-noise and noise reduction of trailing edge (TE) serrations. Interaction of the disturbance with the trailing edge was the main source of self-noise. He also showed that laminar boundary layer separation, laminar-turbulent transition and turbulent reattachment led to additional sources which became dominant at high frequencies, while trailing edge noise was dominant at low frequency.

Doolan *et al.* [2] described the mechanism of trailing edge noise generation. Empirical methods, direct methods and hybrid methods of computing trailing edge noise were also described. The importance of modelling a turbulent flow field for TE noise prediction were discussed. LES, being more accurate than RANS for modelling a turbulent flow field, required better SGS models to be developed if the turbulence scales were smaller than grid size. Different analytical and numerical methods to estimate the noise from turbulent flow data were described.

Jackson *et al.* [3] investigated the airfoil self- and shear-noise for a NACA 0012 airfoil section at three angles of attack. The results were analyzed for the trailing edge noise effects and on how noise sources varied with different angles of attack. A direct correlation between turbulent intensity and the acoustic power level was formulated. Self-noise became more dominant as angle of attack was increased. At larger angles of attack y-sources of self- and shear- noise contributed more as noise compared to the x-sources

In the present study, a supercritical airfoil cross-section was studied at low-Re flow for aero-acoustic parameters such as acoustic power level and LEE noise, and effects of turbulence and vorticity were explained. Angles of attack of 0^0, 6^0 and 12^0 were considered to give a clear idea of the influence of angle of attack on flow noise.

2. Computational Method

2.1 Mathematical Model

The most complete model available for the flow of air is the Navier-Stokes equations. They, however, represent a model, not physical truth. They represent three conservation laws:

Conservation of mass:

$$\frac{\partial(\rho u)}{\partial x}+\frac{\partial(\rho v)}{\partial y}=0 \tag{1}$$

Conservation of momentum:

$$\rho(u\frac{\partial u}{\partial x}+v\frac{\partial u}{\partial y})=-\frac{\partial \rho}{\partial x}+\mu(\frac{\partial^2 u}{\partial x^2}+\frac{\partial^2 u}{\partial y^2}) \tag{2}$$

$$\rho(u\frac{\partial v}{\partial x}+v\frac{\partial v}{\partial y})=-\frac{\partial \rho}{\partial x}+\mu(\frac{\partial^2 v}{\partial x^2}+\frac{\partial^2 v}{\partial y^2}) \tag{3}$$

* Corresponding author. Tel.: +88-01789-908629, +88-01757-001196, +88-01626-501889.
E-mail addresses: angkanhaider@gmail.com, joytanveer796@gmail.com, md.fazlurrahmantonmoy@gmail.com

Conservation of Energy:

$$\frac{\partial(\rho uE)}{\partial x}+\frac{\partial(\rho vE)}{\partial y}=\frac{\partial(\rho uq)}{\partial x}+\frac{\partial(\rho vq)}{\partial y}$$
$$+\frac{\partial}{\partial x}(u\tau_{xx}+v\tau_{xy})+\frac{\partial}{\partial y}(u\tau_{xy}+v\tau_{yy}) \quad (4)$$

2.2 Solver Settings

The solver used was ANSYS Fluent. The settings are given in Table 1.

Table 1 Solver, viscous model and noise sources

Function	Option
Model	*k-ω* (2 equation)
k-ω model	SST
k-ω option	Low Re Corrections
Turbulent Viscosity	None
Options	Viscous Heating Curvature Correction
Solver	Pressure-based
Space	2D
Gradient Option	Least Squares Cell-Based
Formulation	Implicit
Time	Transient
Acoustics	Broadband Noise Sources

3. Computational Domain

The computational domain was discretized with a user-defined structured mesh. The total number of cells used was 96,090. In the wall normal direction, the first node after the wall was selected in such that the value of wall y^+ was around 1. The mesh around the airfoil wall was made dense to ensure higher accuracy.

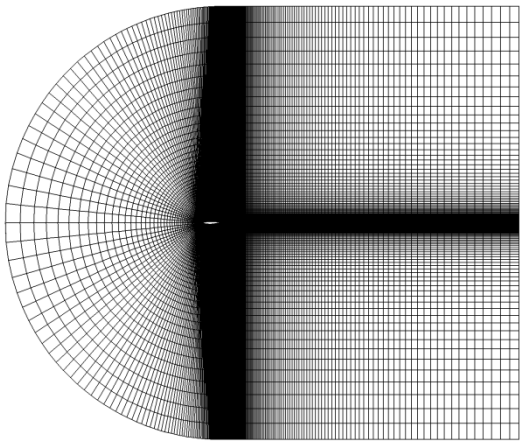

(a) Mesh of the complete domain

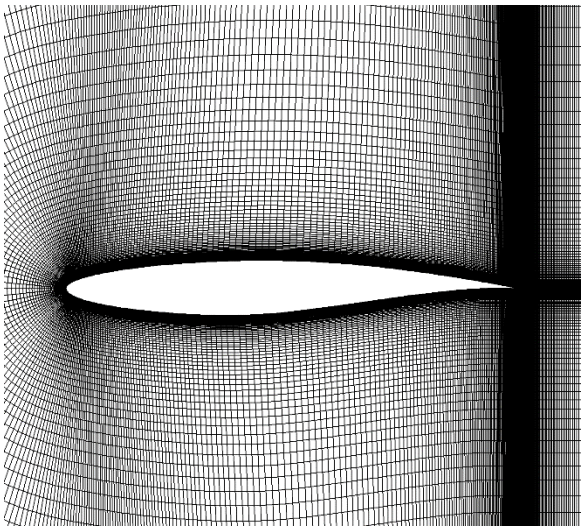

(b) Relatively denser mesh around airfoil

Fig. 1 Discretization and Mesh

4. Boundary Conditions

The boundary of the domain consisted of a domed inlet with velocity of 30 m/s and a pressure outlet. The airfoil surface was taken to be a no-slip wall. The flowing fluid was air with constant density and viscosity at 300K and a Reynolds number of about 168,000 (based on chord length) was maintained. Three different cases of flow were considered by varying the angles of attack. The three angles used were 0^0, 6^0 and 12^0.

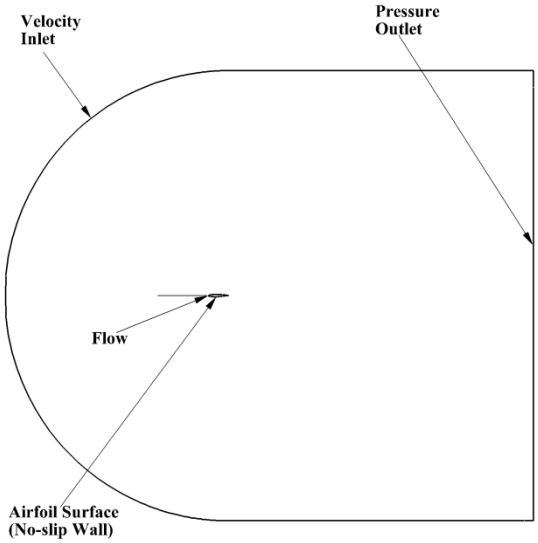

Fig. 2 Boundary Conditions

Table 2 Three cases of flow

Case	Angle of attack
Case – 1	0^0
Case – 2	6^0
Case – 3	12^0

5. Validation of Computational Method

Since very little computational or experimental work is done on supercritical airfoils at low Re, the computational method was validated for a NACA 0012 airfoil profile and pressure coefficient values were compared to those obtained by Jackson *et al.* [3]. As can be seen in Fig. 3, the values obtained were quite reasonable, despite some fluctuations.

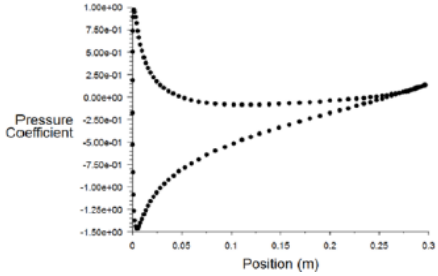

(a) C_p for 10^0 angle of attack (Jackson *et al.*)

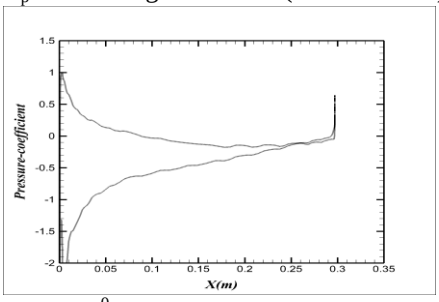

(b) C_p for 10^0 angle of attack (present method)

Fig. 3 Validation of computational method

6. Results and Discussions

The pressure contours for Cases - 1, 2 & 3 angles of attack are shown in Fig. 4. From Fig. 4. (a) and 4. (b), it can be seen that at 0° angle of attack there was an adverse pressure gradient towards the vicinity of Trailing Edge (TE) but at 6° angle of attack adverse pressure gradient occurred just downstream of the Leading Edge (LE). The adverse pressure gradient was correlated with the transition length and the formation of turbulent boundary layer as given by Fahy *et al.* [4]. These phenomena were substantiated by the demonstration of turbulent intensity for 0° and 6° angle of attack (Fig. 6. (a) and 6. (b)) as these figures showed that turbulence started earlier in case of 6° angle of attack in comparison to the case of 0° angle of attack due to separation of flow, resulting in negative pressure at LE for 6^0. At 12° angle of attack vortex shedding occurred which was evident in Fig. 4. (c), characterized by circular negative pressure regions. Turbulent intensity for 12° angle of attack shown in Fig. 6. (c) was in complete agreement with the occurrence of vortex shedding.

The comparison between turbulent intensity in Fig. 6 and contours of acoustic power level in Fig. 5 suggested a direct correlation between them. Both acoustic power level and turbulent intensity increased as the angle of attack was increased.

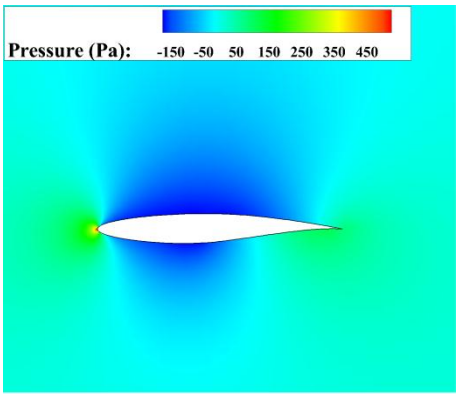

(a) Case - 1

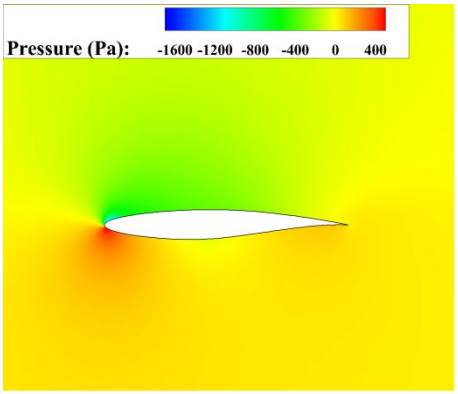

(b) Case – 2

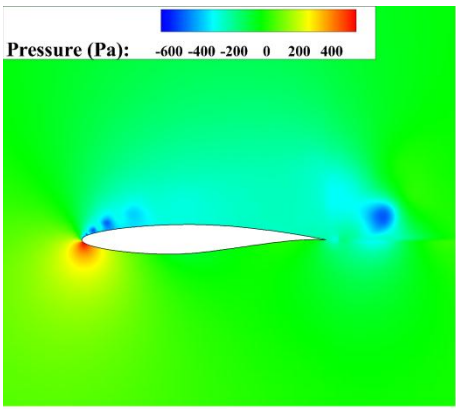

(c) Case - 3

Fig. 4 Pressure Contours at different cases

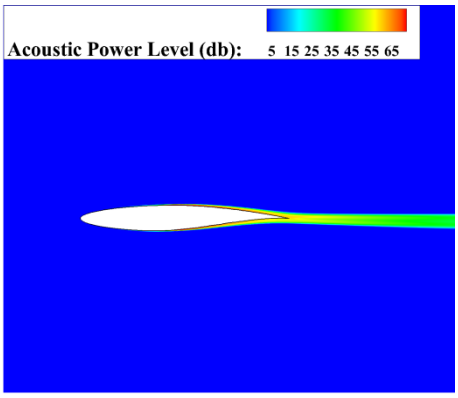

(a) Case - 1

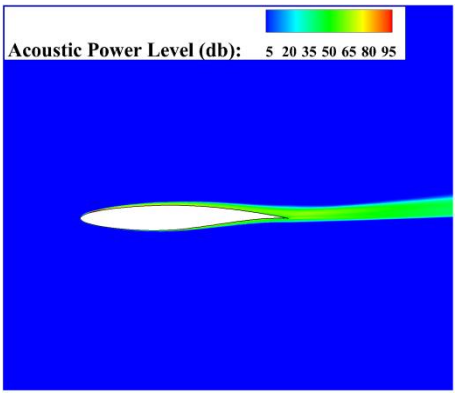

(b) Case – 2

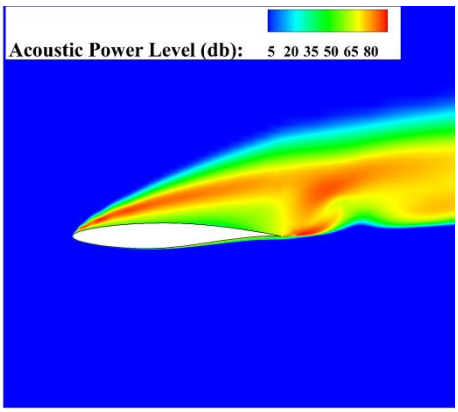

(c) Case – 3

Fig. 5 Contours of Acoustic Power Level

For this study, Broadband Noise Source Model was used to compute aerodynamic noise. Source terms in Linearized Euler Equations (LEE) were used as source model to quantify different sources (self-noise and shear-noise) contributing to the generation of noise. Self-noise arose from the interaction between turbulent fluctuations with the surface of the airfoil and shear-noise arose from the interaction between mean shear and velocity fluctuation as proposed by Crighton *et al.* [5]. Graphs of self-noise and shear-noise sources were plotted for 0°, 6°, 12° angle of attack. It was seen that graphs of x and y sources of self-noise (Fig. 7 & 8) were quite similar for each angle of attack and it indicated that the contribution of x and y sources to the self-noise were almost equal. Even though the pattern of local distribution of x and y sources of shear-noise (Fig. 9 & 10) were quite similar, y-source of shear noise dominated the x-source of shear noise. Increase in angle of attack caused increase in both x and y sources of self-noise and shear-noise. Shear-noise sources were greater than self-noise sources for each angle of attack. But contributions of self-noise sources became higher at higher angle of attack. Both x and y sources of self-noise and shear-noise had higher value near the LE at 6° angle of attack than the values obtained at 12° angle of attack. One possible reason behind this result was that at the end of flow time, a separated low pressure region was generated only at LE for 6^0 but for 12^0 two separate vortices were being shed form the two edges as studied by Lam *et al*. [6], resulting in two peaks, both having lower noise source magnitudes than for the 6^0 case.

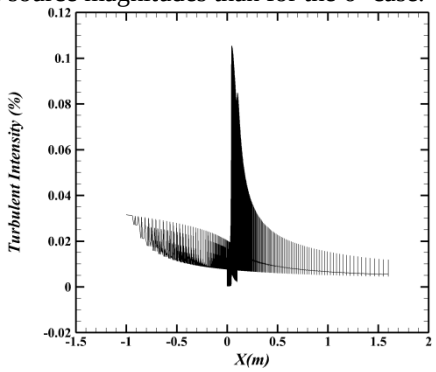

(a) Case – 1

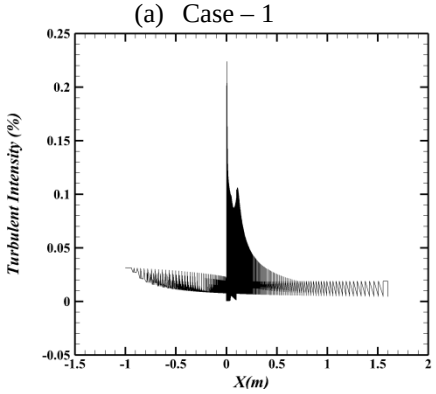

(b) Case – 2

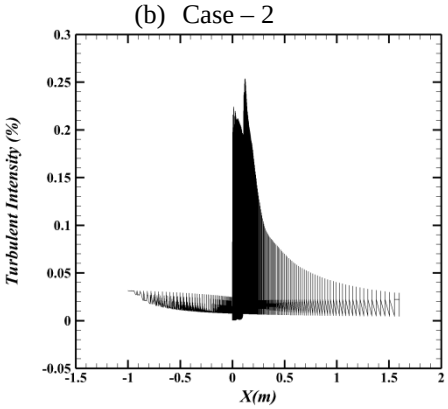

(c) Case -3

Fig. 6 Turbulent intesity at different cases

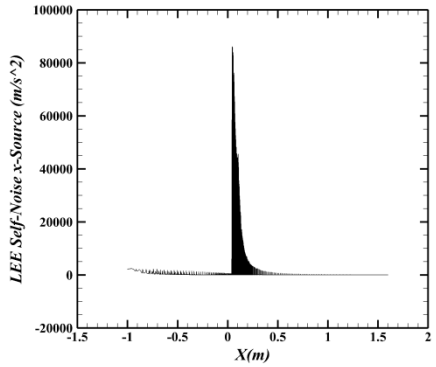

(a) Case – 1

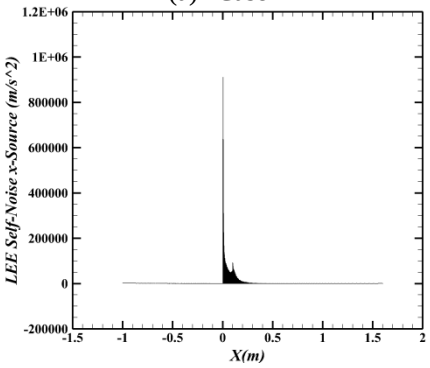

(b) Case – 2

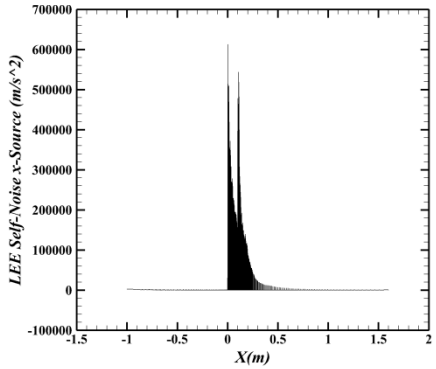

(c) Case – 3

Fig. 7 LEE Self-noise (x-sources) at different cases

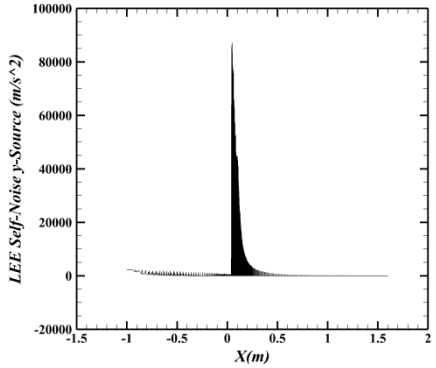

(a) Case – 1

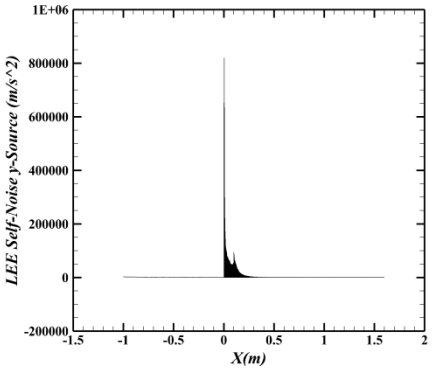

(b) Case – 2

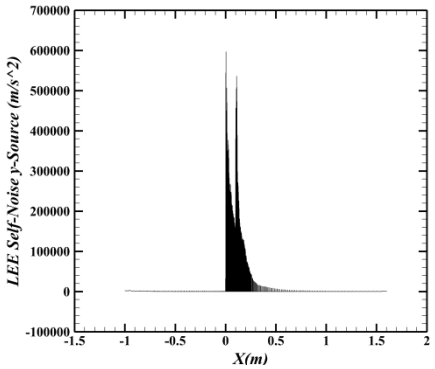

(c) Case – 3

Fig. 8 LEE Self-noise (y-sources) at different cases

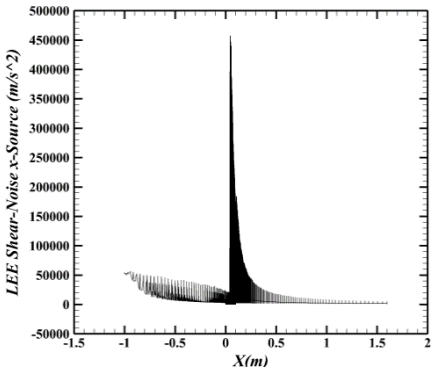

(a) Case - 1

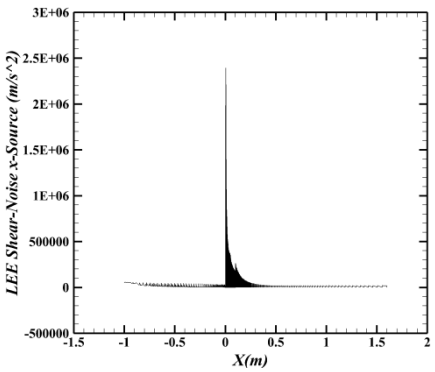

(b) Case – 2

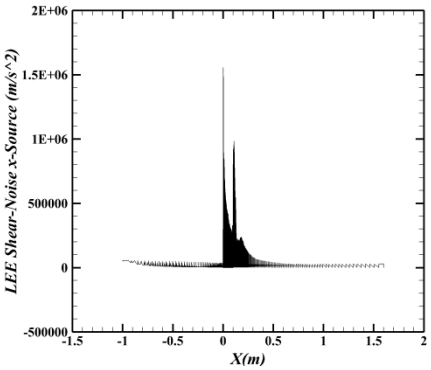

(c) Case – 3

Fig. 9 LEE Shear-noise (x-sources) at different cases

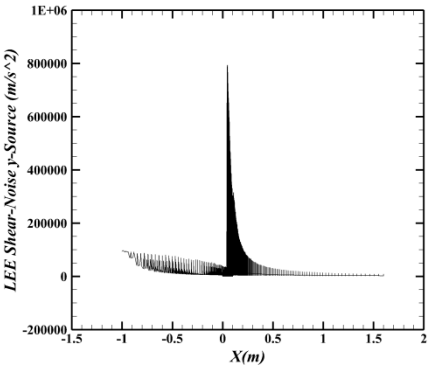

(a) Case – 1

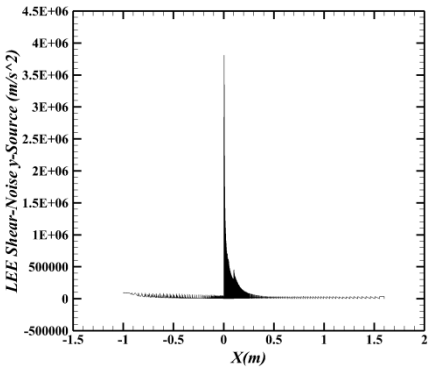

(b) Case – 2

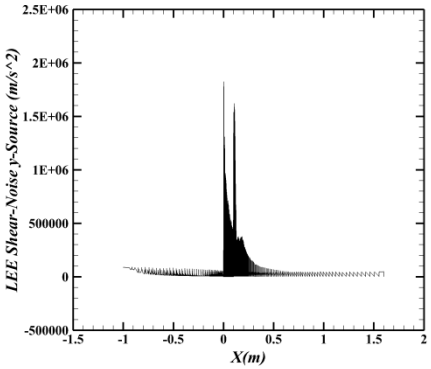

(c) Case – 3

Fig. 10 LEE Shear-noise (y-sources) at different cases

7. Conclusions

In this study, a numerical study of low Reynolds number flow at 3 angle of attack over a supercritical RAE-2822 airfoil cross-section was done.

It was found that with the increase of angle of attack, the acoustic power level increased as a direct result of increase in turbulence with flow separation at the lower angles (0^0 and 6^0) and vortex shedding at higher angle (12^0). For the 6^0, case adverse pressure gradient close to the LE caused flow to separate and become turbulent. Vortex formation and shedding as observed in the 12^0 case introduced greater turbulence and hence more potent noise.

Shear-noise source terms were higher in magnitude compared to self-noise sources for each angle of attack. But contributions of self-noise sources became higher at the higher angle. Both x and y sources of self-noise and shear-noise had higher value near the LE at 6° angle of attack than the values obtained at 12° angle of attack which could be due to the shedding of two separate vortices from both LE and TE for 12^0 as opposed to a single low pressure separated region at the vicinity of the LE for the 6^0 case. This formation of two different vortices also explained the two distinct peaks observed in all the noise source graphs for the 12^0 but only a single peak for the noise source graphs of the 0^0 and 6^0 cases.

REFERENCES

[1] Sandberg, R.D. and Jones, L.E., 2010. Direct numerical simulations of airfoil self-noise. *Procedia Engineering*, *6*, pp.274-282.

[2] Doolan, C., 2008. A review of airfoil trailing edge noise and its prediction.

[3] Jackson, B.R. and Dakka, S.M., 2018. Computational fluid dynamics investigation into flow behavior and acoustic mechanisms at the trailing edge of an airfoil. *Noise & Vibration Worldwide*, *49*(1), pp.20-31.

[4] Fahy, F. and Walker, J. eds., 2004. *Advanced applications in acoustics, noise and vibration*. CRC Press.

[5] Crighton, D.G., 1975. Basic principles of aerodynamic noise generation. *Progress in Aerospace Sciences*, *16*(1), pp.31-96.

[6] Lam, K.M. and Wei, C.T., 2010. Numerical simulation of vortex shedding from an inclined flat plate. *Engineering Applications of computational fluid mechanics*, *4*(4), pp.569-579.